16th Australasian Fluid Mechanics Conference
Crown Plaza, Gold Coast, Australia
2-7 December 2007

Vortex-Induced Vibration of a Neutrally Buoyant Tethered Sphere

Hyeok Lee[1], Mark C. Thompson[1,2] and Kerry Hourigan[1,2]

[1]FLAIR, Department of Mechanical Engineering
Monash University, Melbourne, Victoria, 3800 AUSTRALIA

[2]Division of Biological Engineering
Monash University, Melbourne, Victoria, 3800 AUSTRALIA

Abstract

Recent preliminary experiments have indicated that a neutrally buoyant tethered sphere develops a large diameter quasi-circular trajectory, unlike the oscillations observed for non-neutrally buoyant tethered spheres. This shows similarities to the path of buoyant bubbles, which may follow zig-zag and/or helical paths depending on the Reynolds number. The current study explores the behaviour using well resolved numerical simulations. The forces like tension, buoyancy and fluid force are considered. It is found that there exist six different flow regimes within the range of the Reynolds number = [50, 800] according to the sphere response. Regime I (Re = [50, 205]) and Regime II (Re = [210, 260]) are characterised by steady axisymmetric flow structure without body movement except the loss of axisymmetry in Regime II. The sphere starts to vibrate from Regime III (Re = [270, 280]). Regime IV (Re = [300, 330]) shows suppressed body oscillation and steep decrease of off-centered distance in the plane normal to streamwise direction (yz plane). In Regime V (Re = [335, 550]), the sphere oscillates around (0, 0) in yz plane. The sphere of Regime VI (Re = [600, 800]) oscillates rather irregularly. The transitions are compared with those for a fixed sphere. In addition, the effect of moving away from neutral buoyancy is examined.

Introduction

Vortex-induced vibration (VIV) of structures is of practical interest to many fields of engineering; for example, it can cause vibrations of heat exchanger tubes, and it influences the dynamics These are only a few in a number of problems where VIV is important. The practical significance of VIV has led to a large number of fundamental studies, many of which are discussed in the comprehensive reviews [15, 22]. As the wakes and the vortex shedding patterns of bluff bodies are closely related to VIV, the literature of the sphere at rest is worth to be reviewed. The review of VIV of the tethered bluff bodies follows.

Sphere at Rest

The wake transitions for another widely studied bluff body, the sphere, are remarkably different to those of the circular cylinder [6, 12, 19, 18]. A major difference in the wake transition behaviour of the sphere and the circular cylinder wake is that the sphere wake becomes asymmetrical prior to a transition to unsteady flow, whereas the cylinder wake does not become asymmetrical until the wake goes unsteady [20]. For the sphere wake, the transition from attached to separated flow at the rear of the sphere has been found from direct numerical simulations to be $Re_1 = 20$ [19, 6]. As the Reynolds number increased, the wake remains steady and axisymmetric up to $Re_2 = 211$ [6]. The transition to asymmetry is through a regular bifurcation, i.e. steady to steady flow [19]. Their studies located the transition at $Re_2 = 212$. [6], experimentally and numerically, found the resulting wake to undergo a regular bifurcation through a shift of the steady recirculating bubble behind the sphere from the axis. The remarkable early dye visualizations of Magarvey and Bishop [9] found that a double-threaded wake exists in the range of Re = [200, 350]. Since then, more accurate experiments and numerical simulations have refined this range considerably. These two threads of vorticity trail downstream from the recirculation bubble. This wake structure has also been predicted numerically by Tomboulides and Orszag [19]. The steady asymmetric wake undergoes a further transition to unsteady flow at $Re = 277.5$ as determined by stability analysis [11]. Tomboulides and Orszag [19], and Johnson and Patel [6] support this bifurcation scenario, with unsteady wakes being observed for $Re > 280$. In all cases, the unsteady wake consisted of hairpin-shaped vortex loops shedding downstream from the sphere, in the same plane as that of the initial steady asymmetric structures. The periodic wake of the sphere remains planar-symmetric up to $Re \approx 375$, as observed numerically by Mittal [10].

Tethered Circular Cylinder

One of the simplest extensions to the classical problem of an elastically mounted oscillating cylinder is a circular cylinder whose motion is confined to an arc by a restraining tether. In contrast to the elastically mounted cylinder, little progress has been made regarding the fluid-structure interaction of a tethered body. This system geometry has practical applications in submerged pipelines, offshore spar platforms and light craft tethered in air. It is also of interest because it exhibits flow-induced oscillation where the combined effects of in-line oscillation and transverse oscillation may be observed.

Recently, Ryan *et al.* [14] numerically studied the tethered cylinder system with a spectral element method. It was found that, at large mean layover angles, the tethered cylinder would behave in a fashion similar to the elastically mounted cylinder with low mass ratio and oscillate in either the upper or lower branch of shedding depending on the reduced velocity, U^*, and the mass ratio, m^*. Here, U^* is the flow velocity normalised by cylinder diameter D and frequency of body oscillation f, and m^* is the body mass normalised by the displaced mass of fluid. They noted the cylinder system to be strongly influenced by the mean layover angle, as this parameter determined if the oscillations would be dominated by in-line oscillations, transverse oscillations or a combination of the two. Three branches of oscillation are noted, an in-line branch, a transition branch and a transverse branch. The in-line oscillation for small layover angle corresponds to a classic Karman street wake, and the transverse oscillation for larger layover angle at higher flow speeds corresponds to the formation of vortex pairs. Within the transition branch, the cylinder oscillates at the vortex shedding frequency and modulates the drag force such that the drag signal is dominated by the lift frequency. It was found that the mean amplitude response is greatest when the cylinder is oscillating predominantly transverse to the fluid flow, and the oscillation frequency is synchronized to the vortex shedding frequency of a stationary cylinder, except at very high reduced velocities.

Tethered Sphere

Both numerically and analytically, the tethered cylinder provides a simplification to the fully three-dimensional problem of a tethered sphere. The majority of early work on tethered spheres was concerned with the action of surface waves on tethered buoyant structures [4, 16]. They employed empirically obtained drag and inertia coefficients for use in Morison's equation. The tethered sphere was found to vibrate vigorously due to the waves as expected. However, the coupling of the wave motion and the dynamics of the sphere made it difficult to understand the underlying dynamics of the sphere motion.

The research concerning fully submerged tethered bodies was first examined by Govardhan and Williamson [2] who found that a tethered sphere does indeed vibrate in a uniform flow. In particular, they found that it will oscillate vigorously at a transverse peak-to-peak amplitude of about two diameters. The transverse oscillation frequency was at half the frequency of the in-line oscillations, although the natural frequencies of both the in-line and transverse motions were the same. In the Reynolds number range of their experiments ($Re < 12,000$), the response amplitude was a function of the flow velocity. However, conclusions regarding the synchronization of natural and vortex formation frequencies were lacking due to the large scatter in the literature of the vortex formation frequency in the wake of a sphere. Govardhan and Williamson [2] noted that the maximum root-mean-square (RMS) amplitude was approximately 1.1 diameters, regardless of the mass ratio. It was further found that the vortex shedding frequency for a fixed sphere matched the natural frequency for the tethered sphere at the same reduced velocity, $U^* \approx 5$, at which the local peak in the RMS response occurred. This suggests that the local peak in the RMS response is caused by a resonance between the natural frequency of the tethered body and the wake vortex shedding frequency, and is known as Mode I response. For high mass ratios (typically $m^* \gg 1$), the oscillation frequency at high U^* tended toward the natural frequency. However, it is interesting to note that the oscillation frequency for low mass ratios ($m^* < 1$) at high U^* did not correspond to either the natural frequency or the vortex shedding frequency for a fixed sphere. Through wind tunnel experiments, Jauvtis *et al.* [5] were able to study mass ratios between $m^* = 80$ and $m^* = 940$ and reduced velocities in the range of U^* = [0, 300]. For the sphere of $m^* = 80$, they found a new mode of vibration (which they define as Mode III) and which extends over a broad regime of U^* from 20 to 40.

Govardhan and Williamson [3] extended their previous study on sphere vortex-induced vibration and found that the body oscillation frequency (f) is of the order of the vortex shedding frequency of fixed body (f_{vo}) and there exist two modes of periodic large-amplitude oscillation, defined as modes I and II [2, 21], separated by a transition regime exhibiting non-periodic vibration. In the case of the very light tethered body, the transition between modes is quite distinct, especially when the response amplitude is plotted versus the parameter $(U^*/f^*)St$ which is equivalent to f_{vo}/f, where a jump between modes is clearly exhibited They noted that the phase of the vortex force relative to sphere dynamics is quite different between the modes I and II. This difference in the phase of the vortex force is consistent with the large difference in the timing of the vortex formation between modes, which was observed from the vorticity measurements for the light sphere vibrations. This mode cannot be explained as the classical lock-in effect, since between 3 and 8 cycles of vortex shedding occurs for each cycle of sphere motion. For reduced velocities beyond the regime for Mode III, another vibration mode was discovered that grew in amplitude and persisted to the limit of flow speed in the wind tunnel [5]. The sphere dynamics of this Mode IV were characterized by intermittent bursts of large-amplitude vibration, in contrast to the periodic vibrations of Modes I, II and III.

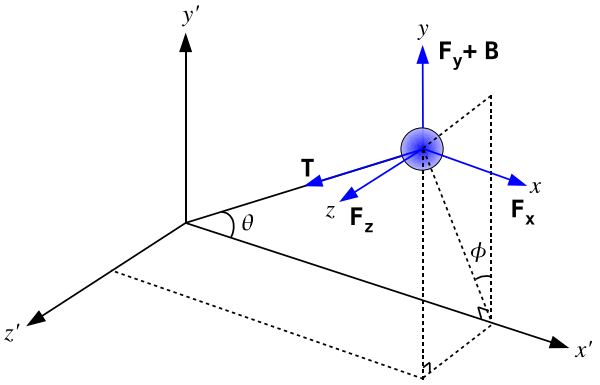

Figure 1: Coordinate system and geometry of tethered sphere and forces

Pregnalato [13] numerically found that a buoyant tethered sphere oscillates at large amplitude over a wide range of reduced velocity, which is similar to the previous studies ([2, 21]). He adopted a spectral element method and a coordinate transform to solve the combined fluid-structure system. Even though the flow is within laminar regime ($Re = 500$), he observed the Modes I, II and III which are shown in [5].

Formulation

The tethered sphere system is descirbed in Figure 1, and the forces acting on the sphere are a tension (T), a buoyancy force (B), the fluid force in the streamwise direction (F_x), the lateral direction (F_y) and the transverse direction (F_z). The tether is assumed to be inextensible, which has been shown to be reasonable within this parameter range by the previous experimental studies. It is also assumed that the tether is attached to the centre of mass, and it has showed negligible effect on the body dynamics as long as the tether length (L) is long enough compared to the size of the body, *e.g.* $L \geq 5D$, where D is diameter of sphere or circular cylinder ([13, 14]).

The tension is linked to the other force components by:

$$T = F_x \cos\theta + (F_y + B)\sin\theta\cos\phi + F_z \sin\theta\sin\phi, \qquad (1)$$

where θ, the tether angle, is the angle between the tether and the streamwise (x) axis, and ϕ is the the inclination angle of the sphere in the phase (yz)plane. For reference, θ plus the layover angle of [14] equals 90^o.

The equations of motion of the sphere are given by:

$$m\ddot{x} = F_x - T\cos\theta, \qquad (2)$$

$$m\ddot{y} = (F_y + B) - T\sin\theta\cos\phi, \qquad (3)$$

$$m\ddot{z} = F_z - T\sin\theta\sin\phi. \qquad (4)$$

The dynamics of a tethered sphere were investigated for mass ratio of $m^* = 1.0$ which is neutrally buoyant. The case of $m^* = 0.91$ was also studied to evaluate the effect of introducing a small degree of buoyancy.

Computational Method

Time Advancement

A high-order, three-step, time-splitting scheme was employed in the solution of the velocity and pressure field. The three steps account for the convection, pressure and diffusion terms of the Navier-Stokes equation. In the first of the three substeps, the convection term was evaluated using a third order Adams-Bashforth scheme and Adams-Moulton scheme. Then, the pressure field was evaluated by forming a Poisson equation by taking the divergence of the equation for the pressure, and enforcing continuity at the end of the substep. The diffusion term was evaluated with the theta form of the Crank-Nicholson scheme. This results in a Helmholtz equation. Both the Poisson equation for the pressure and the Helmholtz equations for the viscous terms lead to linear matrix problems, once the equations are discretised in space. The matrices are inverted at the start of the time-stepping procedure; subsequently, the effects of continuity (pressure) and viscous diffusion at each timestep only involve matrix multiplication. Because the convection term is nonlinear, it is generally treated with an explicit (third-order) Adams-Bashforth method. For the VIV case, there is strong coupling between the fluid and the structural response. The explicit approach becomes unstable and the overall time-stepping has to be treated semi-implicitly. This is done by iterating through the three substeps and structural update until the velocity and pressure fields, and the cylinder motion, converge. Note that except for the first iteration, the advection term is treated by a semi-implicit Adams-Moulton method, which improves the stability. Typically, it takes two or three outer iterations to establish convergence; however, the timestep can generally be chosen to up to an order of magnitude greater than the Courant timestep, which controls the non-iterative approach used for the forced oscillation simulations.

Spatial Discretisation

Fully three dimensional simulation was performed using a spectral element/Fourier spectral method with a global Fourier spectral discretisation in the third dimension, which is the azimuthal direction in the present study. This has been employed previously for the case of the flow past a circular cylinder [8, 17].

The spatial discretisation consists of F equi-spaced planes in the azimuthal direction, each consisting of an identical spectral element mesh in two (streamwise and transverse directions) dimensions. The flow variables are transformed into Fourier space in the azimuthal direction for each node on the spectral element mesh using a fast Fourier transform. This decouples the problem into a set of F Fourier modes which are then solved independently for the linear operators.

The spatial domain in the streamwise and transverse directions was discretised into a number of macro elements, with the majority concentrated in the wake and boundary-layer regions. Some care was taken to construct a near-optimal mesh, and domain size and resolution studies were conducted to validate the predictions. Within each element, the mesh geometry as well as the velocity and pressure fields, were represented by eighth-order tensor-product polynomials associated with Gauss-Lobatto-Legendre quadrature points. Details of the approach and implementation have been provided by Thompson *et al.* [17]. Higher-order boundary conditions in Karniadakis *et al.* [7] are used for the pressure gradient at no-slip boundaries and at the far-field boundaries. At the outlet, the pressure is fixed and the normal velocity gradient is set to zero.

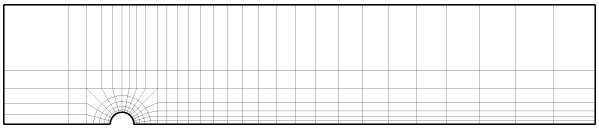

Figure 2: The first mesh used for a tethered sphere system, showing macro element. This mesh is extended along the azimuthal direction with 24 Fourier modes.

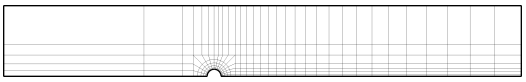

Figure 3: The second mesh used for a tethered sphere system, showing macro element. This mesh is extended along the azimuthal direction with 24 Fourier modes.

Grid Resolution

A grid resolution study was performed to assess the suitability of the mesh used for all of the simulations of the flow past a tethered sphere. At Reynolds number 300, the flow past a stationary sphere is known to be unsteady and characterized by the presence of periodically shed vortices. Based on this, the Reynolds number of 300 was selected, and the Strouhal number (St) was computed to compare the results to the established data from previous studies.

The mesh has $5D$ inlet/side length and $20D$ outlet length and the number of macro elements is 239, as shown in Figure 2.

The resolution of the grid was improved by increasing the order of the polynomial interpolants p (p-refinement in the finite element method) in discrete steps from 5 to 9. Except for $p = 5$, no difference was shown in St over the range of p. The obtained Strouhal number of 0.134 was favorably matched with the value of Johnson and Patel [6] (St = 0.137) and of Tomboulides and Orszag [19] (0.136). Regarding the number of Fourier modes of spectral element method, Ghidersa and Dušek [1] showed that 6 Fourier modes were sufficient in capturing the secondary instability for Re = 275. However, the breaking of planar symmetry for $Re \geq 350$ means that more modes are required to accurately resolve the vortices not only because they shed asymmetrically but also because they are coupled with the motion of the sphere. Therefore, together with the need for additional resolution to handle an increase of Re up to 800, 24 Fourier modes was selected.

To confirm the validity of the choice for the number of Fourier modes, each fluid force coefficient was determined while increasing p from 5 to 9 for 24 Fourier modes. Table 1 shows that $p \geq 6$ is enough to accurately capture the forces acting on the tethered sphere. Considering this result and the expected long computational time for three-dimensional simulations, it was decided that $p = 6$ would be used to simulate the tethered sphere.

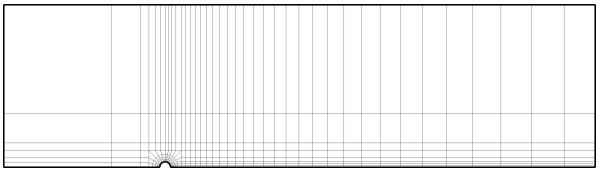

Figure 4: The third mesh used for a tethered sphere system, showing macro element. This mesh is extended along the azimuthal direction with 24 Fourier modes.

p **value**	C_x	C_y	C_z
5	0.679	-0.0207	0.057
6	0.677	0.0025	0.062
7	0.677	0.0027	0.061
8	0.677	0.0027	0.061
9	0.678	0.0028	0.061

Table 1: Streamwise fluid force coefficient C_x, transverse fluid force coefficient C_y and lateral fluid force coefficient C_z with the increase of polynomial interpolant p. The results are for the tethered sphere with m^* = 1.0 and 10D tether length. All coefficients are mean values.

Mesh	r **value**	θ **value**
first (Figure 2)	1.51	4.1
second (Figure 3)	1.52	3.9
third (Figure 4)	1.52	4.1

Table 2: r is the distance from the axis of symmetry (x) to the sphere, and θ is the angle between the tether and x axis. The results are for the tethered sphere with m^* = 1.0 and 10D tether length. All values are mean values.

As well as the previous mesh used, two additional domains have been used for resolution study. The first mesh was the previous mesh shown in Figure 2. The second shown in Figure 3 has 15D inlet length and 22D outlet length, which are longer than those of first one, and 5D sides lengths. The number of macro elements is 251. The third and the largest mesh has 15D inlet/side length and 40D outlet length and has 338 macro elements. This mesh is shown in Figure 4. The resultant mean values of r (*off-centered distance*) and ϕ for the first, second and third mesh have little difference, which is shown in Table 2. This indicates that the first mesh has enough resolution for the tethered sphere simulation. Here, the r is a new parametre defined by $r = \sqrt{y^2 + z^2}$ and is explained more in the next section.

Results

Using the spectral element/Fourier spectral code, the simulations have been performed using high performance computers in the range of Re = [20, 800]. All simulations have been run in parallel to reduced the calculation time, and some simulations have been run over 4000 non-dimensional time units to reach stabilized conditions. For Re = 400 case, the calculation time to compute up to 4000 time units was about 24 hours. The initial Reynolds numbers were chosen in the range of Re = [50, 800] in steps of 50 and intermediate Reynolds numbers between any two neighboring Reynolds numbers were selected if any difference in body dynamics was observed. Re = 205, 210, 270, 280 and 330 are some examples chosen by this process. The tether length was chosen to 10D for all cases. The effect of the tether length will be investigated later. The initial value of θ was set to 5^o and ϕ was to 0^o. These θ and ϕ values were chosen due to the calculation time needed to reach to the converged solution. Several different values of θ (15^o, 30^o, 45^o, and 60^o), and ϕ (5^o and 10^o) have been tested, but needed more time to the converged solutions which showed little difference in the terms of the r, amplitude, and frequency of the sphere.

Off-Centered Distance : r

To quantify the body response, a parameter r is defined and named the *off-centered distance*, which means the distance from the line in the streamwise direction passing through the tether pivot to the centre of the body in yz plane in Figure 1. Because the orientation of vortex shedding for a fixed sphere in uniform flow is quite arbitrary, r is a better quantity than y or z for a neutrally buoyant tethered sphere in which the effect of tension is very small. The mean value r goes to zero if the body moves or oscillates around the axis of symmetry. The r was calculated by $r = \sqrt{y^2 + z^2}$. The body oscillation amplitude and frequency have also been calculated from the r. Figure 5 shows the time averaged (mean) value of r calculated from mean values of y and z.

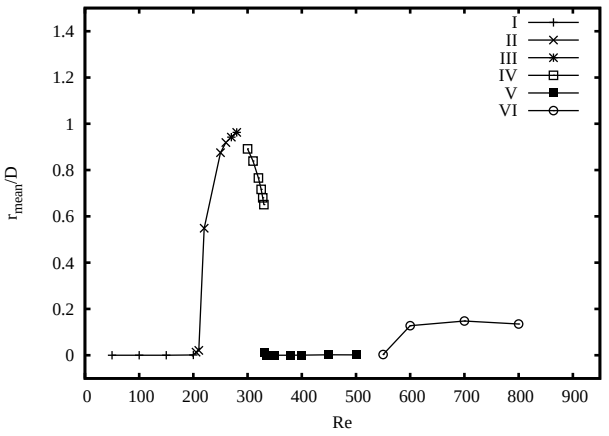

Figure 5: Off-centered distance, r, of neutrally buoyant sphere

Amplitude

It is found that as the Re is increased, the tethered sphere experiences six different flow regimes, which are similar to those of the fixed sphere. The definition of the regimes are determined mainly by the amplitude and the frequency of the body oscillation. In addition, the mean value of r is used to identify the first and the second flow regimes. The first regime (Regime I) is characterised by steady axisymmetric flow structure without body movement. Its Reynolds number range is $Re \leq 205$ based on the Reynolds numbers where the numerical simulations have been made. The sub states of a separation bubble forming at the rear of the body are contained within this regime because they maintained an axisymmetry flow field. The second regime (Regime II) is also steady but with the loss of axisymmetry. The breaking of axisymmetry is observed from Re = 210, and axisymmetry is replaced by planar-symmetry with the appearance of the double-threaded wake. This regime is observed up to Re = 250.

In Regime II, the mean of r increases as Re is increased. As Reynolds number increased further, the sphere starts to vibrate from Re = 270. It was named Regime III. This critical Reynolds number is slightly lower than that of a fixed sphere ($Re \approx 280$ [19]). This trend in critical Reynolds number for a tethered sphere is also observed in the transition to Regime II. The Re is 211 for a fixed sphere [6], and 205 for a tethered one. Regime IV begins at Re = 300. It shows suppressed body oscillation and a steep decrease of the mean of r. In the range of Re = [335, 500] (Regime V), the mean of r goes to zero which means the body oscillates around (0, 0) in the plane normal to stream i.e. yz plane in Figure 1. The amplitude in this regime gradually increases as Re is increased. In Regime VI, the vibrations become chaotic and the sphere undertakes chaotic wandering, having no restoring buoyant forces. The oscillation amplitude becomes less meaningful and very long integration times will be required to determine more precisely the time-mean position of the sphere.

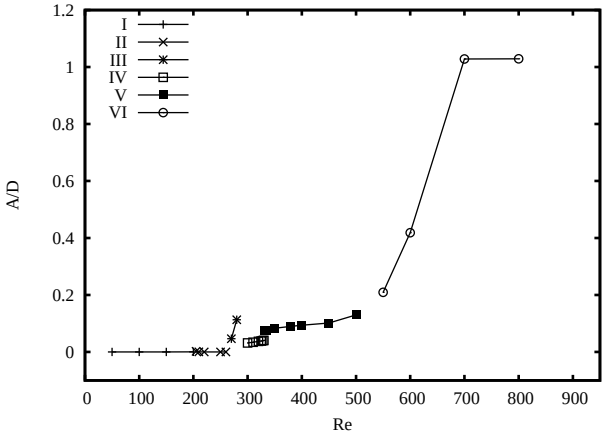

Figure 6: Response of tethered sphere, neutrally buoyant case : Amplitude of *r*

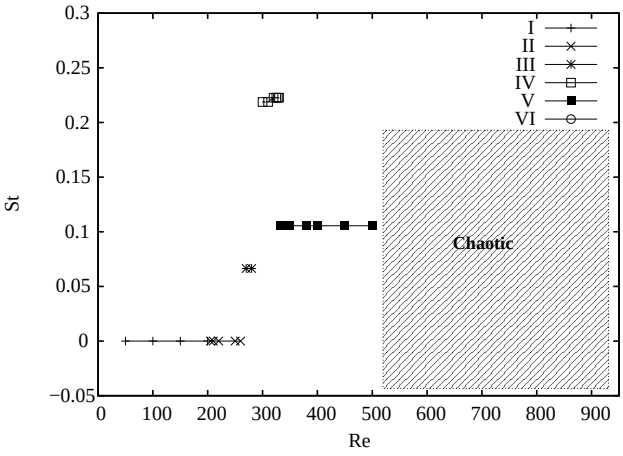

Figure 7: Response of tethered sphere, neutrally buoyant case : Frequency of *r*

Frequency

The frequency response of the sphere is expressed by a Strouhal number (*St*) based on the dominant body oscillation frequency in radial direction (f), freestream velocity (U), and sphere diamater (D). Due to the steady flow of Regime I and II, and the chaotic body motion of Regime VI, the frequencies of Regime III, IV and V are more meaningful in Figure 7. Only the *St* of 0.108 for Regime V is close to (still less than) that of the fixed sphere (*St* = 0.134). The *St* for Regime III is 0.068, and 0.217 for Regime IV.

Trajectory

To identify the vibration shape, the trajectories in yz plane of Regime III, IV and V are investigated. It should be noticed that the orientation of the motion is arbitrary, because the start of vortex shedding for the neutrally buoyant sphere is quite arbitrary. The variation of oscillation amplitudes shown in Figure 6 can be observed in Figure 8 Figure 9. These figures indicate that the shape of the body oscillation of the unsteady regimes is close to straight line except for *Re* = 280 and 500. The difference in two trajectories seems due to the transition between the regimes, as *Re* = 280 and 500 are located at the transition points between Regime III and IV, and Regime V and VI respectivley. In the numerical simulations, those two Reynolds numbers are the last ones of the corresponding regimes.

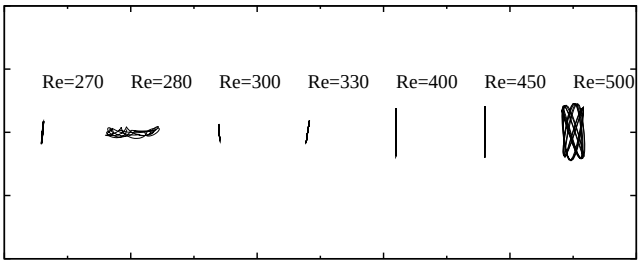

Figure 8: Trajectory in yz plane. Regime III, IV and V. Both axes are of the same scale.

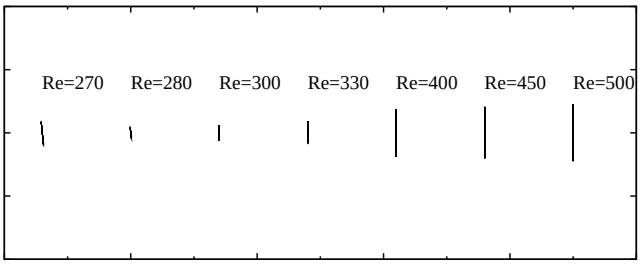

Figure 9: Trajectory in xy plane. Regime III, IV and V. Both axes are of the same scale.

Vortex Structure

The vortex structure of each regime is shown in Figure 10 and Figure 11. The vorticity plot of Regime I is not presented because of its axisymmetry. Figure 10 is the plots of streamwise vorticity. The sphere is off-centred from the axis of symmetry in Regime II although the flow is steady. This is due to the asymmetry of the double-threaded vortex loops. From Regime III, the vortices start to shed periodically, however, the hairpin-shaped vortex loops do not appear as can be seen in the picture corresponding to $Re = 270$ in Figure 10.The hairpin-shaped vortex loops appeared from Regime IV. For the regimes where the hairpin vortex loops appear, the Hussain field is shown in Figure 11 to identify the difference of the loops between the regimes. It seems that these vortex loops maintain their planar-symmetry in Regime IV, but begin to lose the symmetry within Regime V. The sphere in Regime VI (*Re* = 550) shows irregular behaviour and a vorticity contour is shown in Figure 11. After the flow become irregular, the difference in the vortex sturucture is hard to identify.

Conclusions

It is found that there exist six different flow regimes within the range of the Reynolds number = [50, 800]. Regime I (*Re* = [50, 205]) shows steady axisymmetry flow structure without body movement. Regime II (*Re* = [210, 260]) is also characterised by steady flow structure except the loss of axisymmetry. The sphere starts to oscillate at Regime III (*Re* = [270, 280]). Regime IV (*Re* = [300, 330]) shows suppressed body oscillation and the off-centered distance decreases rapidly. In Regime V (*Re* = [335, 550]), the sphere vibrates around (0,0) in yz plane. In Regime VI (*Re* = [600, 800]), the sphere oscillates rather irregularily at larger amplitude than other regimes. Of note is that, in spite of some similarity, the transitions between regimes appear at lower Reynolds numbers than those for the fixed sphere.

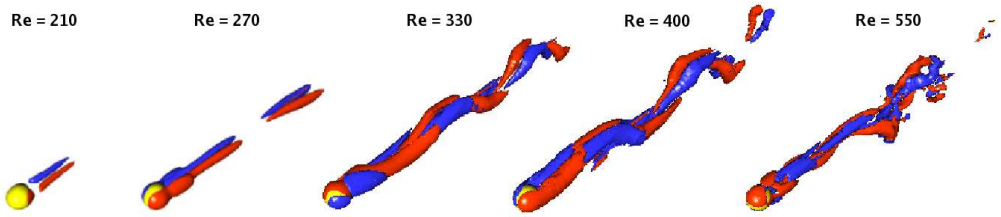

Figure 10: Streamwise vorticity. Each picture corresponds to Regime II, III, IV, V and VI from the left.

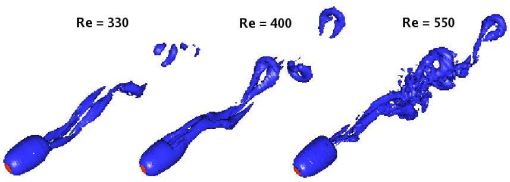

Figure 11: Hussain field. Each picture corresponds to Regime IV, V and VI from the left.

Acknowledgements

This work was supported by the Australian Partnership for Advanced Computing (APAC).

References

[1] Ghidersa, B. and Dušek, J., Breaking of axixsymmetry and onset of unsteadiness in the wake of a sphere, *J. Fluid Mech.*, **423**, 2000, 33–69.

[2] Govardhan, R. and Williamson, C. H. K., Vortex-induced motions of a tethered sphere, *J. Wind Eng. Ind. Aerodyn.*, **69-71**, 1997, 375–385.

[3] Govardhan, R. and Williamson, C. H. K., Vortex-induced vibrations of a sphere, *J. Fluid Mech.*, **531**, 2005, 11–47.

[4] Harlemann, D. and Shapiro, W., The dynamics of a submerged moored sphere in oscillatory waves, *Coastal Eng.*, **2**, 1961, 746–765.

[5] Jauvtis, N., Govardhan, R. and Williamson, C. H. K., Multiple modes of vortex-induced vibrations of a sphere, *J. Fluids Struct.*, **15**, 2001, 555–563.

[6] Johnson, T. A. and Patel, V. C., Flow past a sphere up to a Reynolds number of 300, *J. Fluid Mech.*, **378**, 1999, 19–70.

[7] Karniadakis, G. E., Israeli, M. and Orszag, S. A., High-order splitting methods of the incompressible Navier-Stokes equations, *J. Comp. Phys.*, **97**, 1991, 414–443.

[8] Karniadakis, G. E. and Triantafyllou, G. S., Three-dimensional dynamics and transition to turbulence in the wake of bluff objects, *J. Fluid Mech.*, **238**, 1992, 1–30.

[9] Magarvey, R. and Bishop, R., Wakes in liquid-liquid systems, *Phys. Fluids*, **4**, 1961, 800–805.

[10] Mittal, R., Planar symmetry in the unsteady wake of a sphere, *AIAA J.*, **37**, 1999, 388–390.

[11] Natarajan, R. and Acrivos, A., The instability of the steady flow past spheres and disks, *J. Fluid Mech.*, **254**, 1993, 323–344.

[12] Ormières, D. and Provansal, M., Transition to turbulence in the wake of a sphere, *Phys. Rev. Lett.*, **83**, 1999, 80–83.

[13] Pregnalato, C. J., *The Flow-Induced Vibrations of a Tethered Sphere*, Ph.D. thesis, Monash University, Melbourne, Australia, 2003.

[14] Ryan, K., Pregnalato, C. J., Thompson, M. C. and Hourigan, K., Flow-induced vibrations of a tethered circular cylinder, *J. Fluids Struct.*, **19**, 2004, 1085–1102.

[15] Sarpkaya, T., A critical review of the intrinsic nature of vortex-induced vibrations, *J. Fluids Struct.*, **19**, 2004, 389–447.

[16] Shi-Igai, H. and Kono, T., Study on vibration of submerged spheres caused by surface waves, *Coastal Engineering Japan*, **12**, 1969, 29–40.

[17] Thompson, M. C., Hourigan, K. and Sheridan, J., Three-dimensional instabilities in the wake of a circular cylinder, *Exp. Therm. Fluid Sci.*, **12**, 1996, 190–196.

[18] Thompson, M. C., Leweke, T. and Provansal, M., Kinematics and dynamics of sphere wake transition, *J. Fluids Struct.*, **15**, 2001, 575–585.

[19] Tomboulides, A. G. and Orszag, S. A., Numerical investigation of transitional and weak turbulent flow past a sphere, *J. Fluid Mech.*, **416**, 2000, 45–73.

[20] Williamson, C. H. K., The existence of two stages in the transition to three-dimensionality of a cylinder wake, *Phys. Fluids*, **31**, 1988, 3165–3168.

[21] Williamson, C. H. K. and Govardhan, R., Dynamics and forcing of a tethered sphere in a fluid flow, *J. Fluids Struct.*, **11**, 1997, 293–305.

[22] Williamson, C. H. K. and Govardhan, R., Vortex-induced vibrations, *Ann. Rev. Fluid Mech.*, **36**, 2004, 413–455.